Topologically protected unidirectional edge spin waves and beam splitter

X. S. Wang,[1,2] Ying Su,[2,3] and X. R. Wang[2,3,*]

[1]*School of Microelectronics and Solid-State Electronics, University of Electronic Science and Technology of China, Chengdu, Sichuan 610054, China*

[2]*Department of Physics, The Hong Kong University of Science and Technology, Clear Water Bay, Kowloon, Hong Kong*

[3]*HKUST Shenzhen Research Institute, Shenzhen 518057, China*

(Received 4 October 2016; revised manuscript received 14 January 2017; published 31 January 2017)

Magnetic topological states are investigated theoretically and numerically. It is shown that ferromagnetically interacting spins on a two-dimensional honeycomb lattice with nearest-neighbor interactions, which is governed by the Landau-Lifshitz-Gilbert equation, can be topologically nontrivial with gapped bulk spin waves and topologically protected gapless edge spin waves. These edge spin waves are robust against defects and perturbations, and should be superb channels of processing and manipulating spin waves, in contrast to the normal spin waves that are very sensitive to defects as well as sample geometry. Because of the unidirectional nature of these topologically protected edge spin waves, a spin-wave beam splitter can be made out of a domain wall in a strip. It is shown that an incoming spin-wave beam along one edge splits into two spin-wave beams propagating along two opposite directions on the other edge after passing through a domain wall.

DOI: 10.1103/PhysRevB.95.014435

I. INTRODUCTION

Topological matters have attracted enormous attention in recent years because of their interesting and exotic properties [1–4]. One such property is the existence of unidirectional and topologically protected surface/edge states that are robust against internal and external perturbations. The study was initially exclusive for electron systems and was believed to be a quantum phenomenon. It is now known that the topological states can exist in classical mechanics [5] and photonics [6]. There has also been intensive research on topological magnetic states in recent years [7–22]. Topological magnetic states should be very useful for magnonics that is about generation, detection, and manipulation of magnons [23–26].

Magnetic materials are highly correlated spin systems that do not respect time-reversal symmetry. The low-energy excitations of magnetic materials are spin waves, or magnons. Magnons are promising information carriers in spintronics due to their low energy consumption and long coherence distance, as well as a control knob of magnetization dynamics [27–29]. Topologically protected edge spin waves of a magnetic topological matter can propagate unidirectionally and be insensitive to the system variations. So far, most studies of topological magnetic states [7–19] have started from the Schrödinger equation that is relevant to the phenomena of quantum magnetism including the spin Hall effect while the magnetization in the most magnonic devices is governed by the classical Landau-Lifshitz-Gilbert (LLG) equation. Those studies based on the LLG equation [20–22] focus mainly on the magnetostatic spin waves [30], important for spin waves of long wavelength but with limited applications in magnonic devices. From a practical point of view, the exchange spin waves, the subject of the current paper, shall be more interesting in device applications. In this paper, we show that ferromagnetic spins on a two-dimensional (2D) honeycomb lattice in the presence of a proper nearest-neighbor (NN) exchange interaction, the magnetization dynamics of which is governed by the classical nonlinear LLG equation, can be a magnonic topological matter the spin waves of which are gapped in the bulk and gapless on the edges. Because the bulk spin-wave bands carry nontrivial Chern numbers, the gapless edge spin waves are topologically protected and unidirectional (chiral), which always propagate counterclockwise with respect to the magnetization direction. A staggered sublattice anisotropy can change the system from topologically nontrivial to trivial, and vice versa. The existence and robustness of the edge states are verified by numerically solving the LLG equation. A spin-wave beam splitter based on the edge states in a domain-wall structure is demonstrated.

II. MODEL AND METHODOLOGY

We consider ferromagnetic spins on a 2D honeycomb lattice as shown in Fig. 1(a). $\mathbf{a}_{1(2,3)}$ are three neighboring site vectors of length a. The blue and red arrows represent the magnetic moments $\boldsymbol{\mu}_i = \mu \mathbf{m}_i$ of magnitude μ and direction $\mathbf{m}_i$ on site i of sublattices A and B, respectively. The system is described by a classical Hamiltonian,

$$\mathcal{H} = -\frac{J}{2}\sum_{\langle i,j\rangle} \mathbf{m}_i \cdot \mathbf{m}_j - \frac{1}{2}\sum_{\langle i,j\rangle} \mathcal{F}(\mathbf{m}_i, \mathbf{m}_j, \mathbf{e}_{ij}) - \sum_i \frac{K_i}{2} m_{iz}^2 - \mu B \sum_i m_{iz}, \quad (1)$$

where $\langle i,j\rangle$ denotes the NN sites. The first two terms are, respectively, constant NN exchange interaction of exchange constant J and a NN interaction that depends on $\mathbf{m}_i$, $\mathbf{m}_j$, and the unit vector $\mathbf{e}_{ij}$ connecting sites i and j. In this paper, we consider a NN interaction which takes the form $\mathcal{F}(\mathbf{m}_i, \mathbf{m}_j, \mathbf{e}_{ij}) = F(\mathbf{m}_i \cdot \mathbf{e}_{ij})(\mathbf{m}_j \cdot \mathbf{e}_{ij})$, where F is the interaction strength. This dipole-dipole-like term is usually called the pseudodipolar exchange interaction that can arise from the superexchange and atomistic spin-orbit interaction [31,32]. The third term is the anisotropy energy with the easy axis

*Corresponding author: phxwan@ust.hk

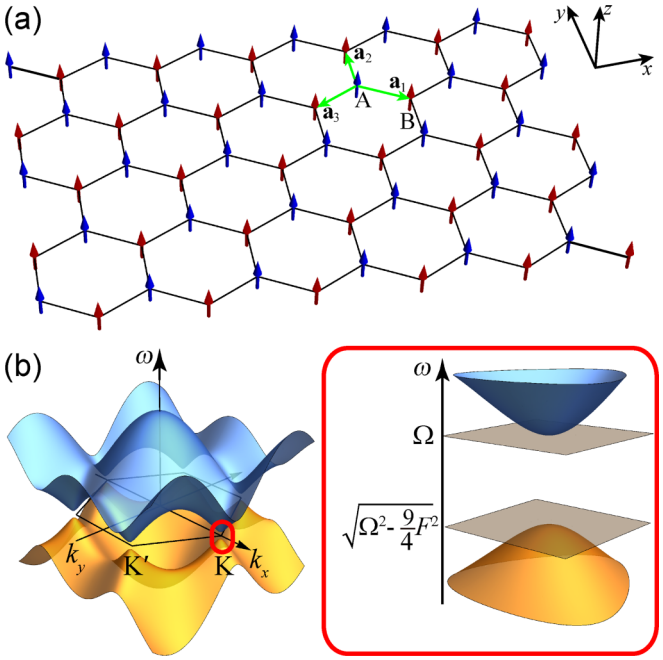

FIG. 1. (a) Schematic diagram of ferromagnetic spins on a honeycomb lattice with perpendicular anisotropy (along z direction). The blue and red arrows denote magnetic moment vectors on A and B sublattices. The green arrows are three neighboring site vectors $\mathbf{a}_{1,2,3}$. (b) The left panel is the spin-wave spectrum of an infinite system in the first Brillouin zone (hexagon shape) for $J = 0.1$, $F = 0.5$, and $\Omega = 1.3$ (in units of $\mu_0\mu^2/a^3$). The right panel is a closeup view of the gap at the K point (indicated by the red circle in the left panel).

along z direction and anisotropy constant $K_i = K_\mathrm{A}$, K_B for sublattices A and B. The last term is the Zeeman energy from a magnetic field B along z direction. For $K_\mathrm{A} = K_\mathrm{B} = K$, the single-domain ferromagnetic state along z direction is a stable state when $\mu B + K > |\frac{3}{2}F|$.

III. RESULTS AND DISCUSSIONS

In the absence of damping, the LLG equation [33] for $\mathbf{m}_i$ becomes

$$\frac{\partial \mathbf{m}_i}{\partial t} = -\mathbf{m}_i \times \left[J\sum_j \mathbf{m}_j + F\sum_j (\mathbf{m}_j \cdot \mathbf{e}_{ij})\mathbf{e}_{ij} + Km_{iz}\mathbf{e}_z + B\mathbf{e}_z \right], \quad (2)$$

where $\mathbf{e}_z$ is the unit vector along z direction. The length, time, magnetic field, and energy are in units of a, $a^3(\gamma\mu)^{-1}$, $\mu_0\mu/a^3$, and $\mu_0\mu^2/a^3$, where γ and μ_0 are, respectively, the gyromagnetic ratio and the vacuum permeability. To obtain the spin-wave spectrum, we consider a small deviation of $\mathbf{m}_i$ from $\mathbf{m}_0 = \mathbf{e}_z$, $\mathbf{m}_i = (\delta m_{ix}, \delta m_{iy}, 1)$, $(\sqrt{\delta m_{ix}^2 + \delta m_{iy}^2} \ll 1)$. The eigensolutions of linearized Eq. (2) have the forms of $\delta m_{ix} = X_\mathrm{A} e^{i(\mathbf{k}\cdot\mathbf{R}_\mathrm{A} - \omega t)}$, $\delta m_{iy} = Y_\mathrm{A} e^{i(\mathbf{k}\cdot\mathbf{R}_\mathrm{A} - \omega t)}$ and $\delta m_{ix} = X_\mathrm{B} e^{i(\mathbf{k}\cdot\mathbf{R}_\mathrm{B} - \omega t)}$, $\delta m_{iy} = Y_\mathrm{B} e^{i(\mathbf{k}\cdot\mathbf{R}_\mathrm{B} - \omega t)}$ for sublattices A and B, where the Bloch theorem is used. We define $\psi_\mathrm{A}^{\pm} = (X_\mathrm{A} \pm iY_\mathrm{A})/\sqrt{2}$, $\psi_\mathrm{B}^{\pm} = (X_\mathrm{B} \pm iY_\mathrm{B})/\sqrt{2}$. From Eq. (2), the equation for the column vector $\Psi(\mathbf{k}) = (\psi_\mathrm{A}^+, \psi_\mathrm{A}^-, \psi_\mathrm{B}^+, \psi_\mathrm{B}^-)^\mathrm{T}$ is

$$H(\mathbf{k})\Psi(\mathbf{k}) = \omega(\mathbf{k})\Psi(\mathbf{k}); \quad (3)$$

$H(\mathbf{k})$ is a 4×4 matrix of the expression

$$H = \begin{pmatrix} \Omega_\mathrm{A} & 0 & -f(\mathbf{k}) & g_1(\mathbf{k}) \\ 0 & -\Omega_\mathrm{A} & -g_2(\mathbf{k}) & f(\mathbf{k}) \\ -f^*(\mathbf{k}) & g_2^*(\mathbf{k}) & \Omega_\mathrm{B} & 0 \\ -g_1^*(\mathbf{k}) & f^*(\mathbf{k}) & 0 & -\Omega_\mathrm{B} \end{pmatrix}, \quad (4)$$

where $\Omega_\alpha = K_\alpha + B + 3J$, $f(\mathbf{k}) = (J + \frac{F}{2})\sum_j e^{i\mathbf{k}\mathbf{a}_j}$, $g_1(\mathbf{k}) = \frac{F}{2}\sum_j e^{2i\theta_j} e^{i\mathbf{k}\cdot\mathbf{a}_j}$, and $g_2(\mathbf{k}) = \frac{F}{2}\sum_j e^{-2i\theta_j} e^{i\mathbf{k}\cdot\mathbf{a}_j}$ ($\alpha = \mathrm{A,B}$; $j = 1,2,3$); and θ_j is the angle between $\mathbf{a}_j$ and $\mathbf{e}_x$. The solutions come in pairs $\pm\lambda$. Two positive solutions, corresponding to counterclockwise spin precession around their ground states, are relevant (the other two negative solutions are for clockwise spin precession around the local maximal state). Although H is not Hermitian, H can be expressed as SH_1 where H_1 is Hermitian and $S = \sigma_0 \bigotimes \sigma_3$ (with σ_0 being the 2×2 identity matrix and σ_3 the Pauli matrix), and all the eigenvalues of H are real as long as the ferromagnetic state is a stable equilibrium state [34]. The spin-wave dispersion relation $\omega(\mathbf{k})$ is shown in Fig. 1(b) for $J = 0.1$, $F = 0.5$, $K_\mathrm{A} = K_\mathrm{B} = K$, and $\Omega \equiv 3J + K + B = 1.3$ (in units of $\mu_0\mu^2/a^3$). The band gap at K and K′ points is $\Delta_g = \Omega - \sqrt{\Omega^2 - 9F^2/4}$, as shown in the right panel of Fig. 1(b). When $F = 0$, the bands linearly cross each other at K and K′ to form Dirac cones, similar to electron Dirac cones in graphene [35]. Thus, the pseudodipolar NN exchange interaction plays a crucial role in the band-gap opening.

We consider now a long strip of width $100a$ with zigzag edges along x direction as shown in Fig. 1(a). The density plot of the spectral function on the top edge is shown in Fig. 2(a), for the same parameters as those in Fig. 1(b). The negative

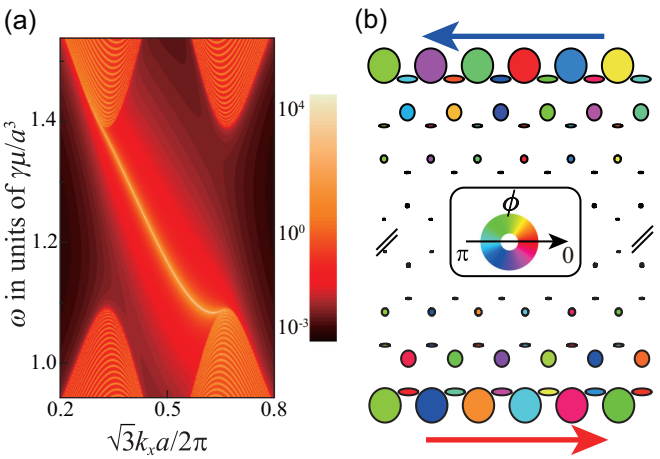

FIG. 2. (a) Density plot of the spectral function on the top edge. Gapless edge spin-wave states are clearly shown in the band gap. The colors (from dark to bright) encode the value of the spectral function (from small to large) in logarithmic scale shown by the color bar. (b) Spatial distribution of the spin-wave edge eigenstate of $\omega = 1.2$ ($\gamma\mu/a^3$). The symbol shape traces the spin precession trajectories, and the size of symbols denotes the amplitude of the spin wave at each site. The azimuthal angles of spins on the lattice at $t = 0$ are encoded by the symbol colors with the color ring shown in the inset.

slope of the dispersion curve (bright line) of the top edge states in the band gap proves that these states propagate to the left. Similarly, the states on the bottom edge propagate unidirectionally to the right. The edge channels connect the upper and lower bands and linearly cross each other in the momentum space. Figure 2(b) shows spatial distribution of the edge spin-wave eigenstate of $\omega = 1.2$ ($\gamma\mu/a^3$). The symbol shapes and sizes are the spin precession trajectory and the precession radius at each site, respectively. The azimuthal angle ϕ of $\mathbf{m}$ at $t = 0$ is encoded by the colors with the color ring shown in the inset. It is evident that the spin wave is mainly localized on the outermost sites. Interestingly, the precession trajectories of spins on the outmost sites are almost perfect circles, while those on the other sublattice are ellipses with very high ellipticity and very small amplitudes. In summary, two edge channels separately located on the top and the bottom edges linearly cross each other in the momentum space and end at two valleys. Also, the existence of the unidirectional edge states does not depend on the type of strip edges.

The observed features resemble those of electronic topological insulators with nontrivial topological orders in the bulk. To prove the topological nature of the observed edge states in the present ferromagnetic system, we evaluate the Chern numbers of the spin-wave bulk bands by using a gauge-invariant formula [36],

$$\mathcal{C} = \frac{i}{2\pi}\iint dk_x dk_y \mathrm{Tr}\left[P\left(\frac{\partial P}{\partial k_x}\frac{\partial P}{\partial k_y} - \frac{\partial P}{\partial k_y}\frac{\partial P}{\partial k_x}\right)\right], \quad (5)$$

where P is the projection matrix $P(\mathbf{k}) = \Psi(\mathbf{k})\Psi(\mathbf{k})^\dagger$. $\Psi(\mathbf{k})$ is the normalized eigenstate of wave vector $\mathbf{k}$, and the integration is over the first Brillouin zone. As long as $F \neq 0$, the Chern number of the lower band is $+1$ and that of the upper band is -1, consistent with the theorem that the sum of the Chern numbers of all bands must be zero [37]. The unidirectional spin-wave edge states are similar to the chiral electron edge states in the quantum Hall and quantum anomalous Hall systems, and are robust against disorders. This nontrivial topological order can only be destroyed by closing and reopening the band gap. To see this, we let sublattices A and B have different anisotropy constants of $K_A = K - \Delta$ and $K_B = K + \Delta$, respectively. The band gap at the K point is in the range of $\sqrt{\Omega^2 - 9F^2/4} + \Delta < \omega < \Omega - \Delta$, while the band gap at the K′ point is in the range of $\sqrt{\Omega^2 - 9F^2/4} - \Delta < \omega < \Omega + \Delta$. If we gradually increase (decrease) Δ from zero, the band gap at the K (K′) point shrinks and the gap closes at $\Delta = \Delta_g/2$ ($-\Delta_g/2$), where $\Delta_g = \Omega - \sqrt{\Omega^2 - 9F^2/4}$. With further increase (decrease) of Δ, the gap reopens and the whole spectrum becomes fully gapped without topologically protected edge states. Figure 3 shows the band structures of zigzag strips for $\Delta = 0$, $\Delta_g/2$, and $0.63\Delta_g$, with other parameters being the same as those in Figs. 1 and 2. The Chern numbers of the corresponding bulk bands are also given. For $|\Delta| < \Delta_g/2$, the edge states cross each other inside the gap in the momentum space, and the topological order is nontrivial, with Chern numbers $\mathcal{C} = \pm 1$ for the lower and upper bands. For $|\Delta| > \Delta_g/2$, the system is topologically trivial with Chern numbers $\mathcal{C} = 0$ for both lower and upper bands. In the topologically trivial case, the edge states could still exist, but do not cross each other, and are not topologically protected.

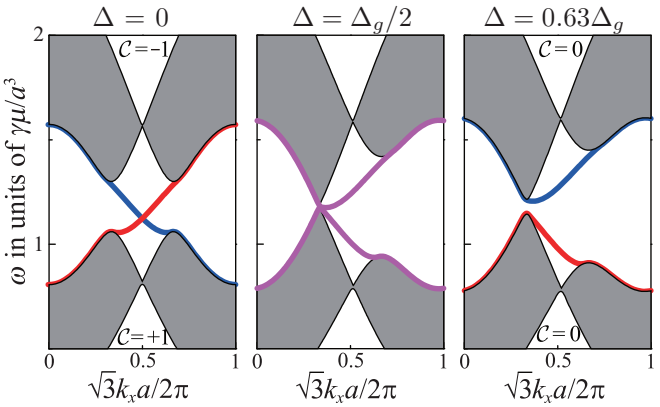

FIG. 3. Spin-wave band structures of a zigzag strip for different Δ ($\Delta = 0$, $\Delta_g/2$, and $0.63\Delta_g$ from left to right, respectively). The gray areas are the bulk states and the color thick lines are the edge states. The Chern numbers of the corresponding bulk bands are given for $\Delta = 0$ and $0.63\Delta_g$.

To study dynamical properties of bulk spin waves and edge spin waves, we numerically solve Eq. (2) on a strip of $20\sqrt{3}a$ long and $14a$ wide. In order to see whether the edge states are robust against defects, we introduce an irregular edge to the sample as shown in Figs. 4(a) and 4(b). To excite spin waves, we apply a circularly polarized microwave field pulse of $\mathbf{h} = h[\cos(\omega t)\mathbf{e}_x + \sin(\omega t)\mathbf{e}_y]$ in a time duration of $0 \leqslant t \leqslant 50$, at the middle site of the top edge indicated by the black arrows in Figs. 4(a) and 4(b). For $h = 0.01$ (μ/a^3) and $\omega = 1.2$ (inside the bulk band gap), Fig. 4(a) shows the snapshots of spin-wave distributions at various times of $t = 50$, 100, 200. The size of the circles is proportional to the local spin-wave amplitude of $\sqrt{m_x^2 + m_y^2}$, and the color encodes the azimuthal angle ϕ. It is apparent that an edge mode is excited and is propagating counterclockwise along the sample edges. Backward scattering and leakage into the bulk can hardly be observed. For a comparison, we also excite spin waves of $\omega = 2$ that are inside the upper bulk band. The snapshots of spatial distributions of the excited spin waves at various times of $t = 10$, 30, 50 are shown in Fig. 4(b). Clearly, the spin wave propagates into the whole sample. New functional devices such as diodes and circulators can be designed by using the unidirectional spin-wave edge states. Below, we propose a spin-wave beam splitter based on the unidirectional edge spin waves in a strip of $40\sqrt{3}a \times 9.5a$ with a domain wall in the middle as shown in Fig. 4(c). The reddish and greenish regions denote two domains with spins pointing to $+z$ and $-z$ directions, respectively. For $J = 0.1$, $K = 1$, and $F = 0.5$ ($\mu_0\mu^2/a^3$), the domain-wall width is less than a. Since the topologically protected edge spin waves propagate counterclockwise in the reddish domain and clockwise in the greenish domain, a spin wave of $\omega = 1.2$, generated on the left bottom edge at the site indicated by the black arrow by a 50-long microwave pulse, propagates rightwards along the bottom edge and reaches the domain wall at $t = 50$ (upper panel). Because no backward (forward) edge spin waves exist on the bottom edge of the reddish (greenish)

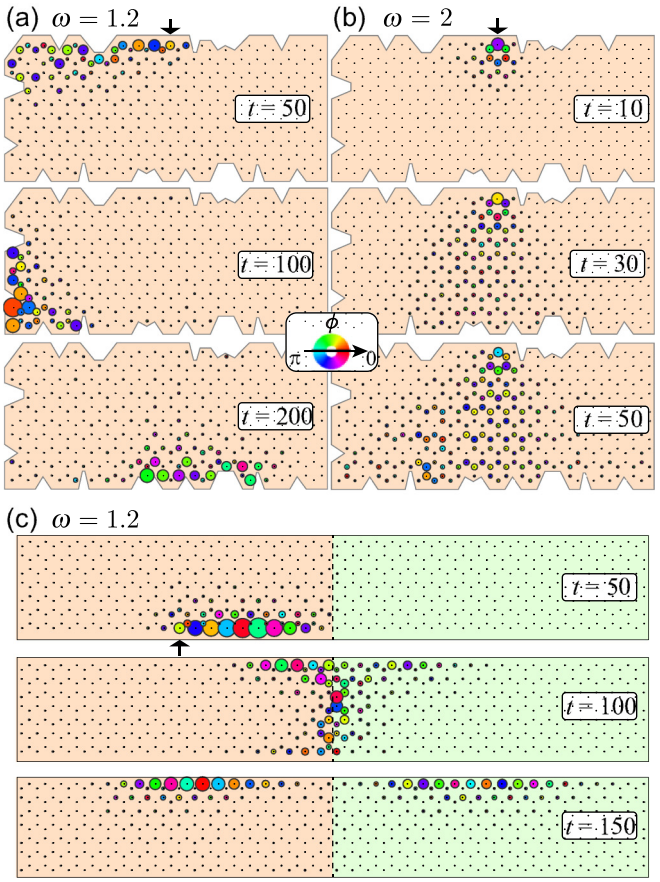

FIG. 4. (a),(b) Snapshots of spatial distributions of the spin waves generated by a microwave pulse of $\Delta t = 50$ long in a $20\sqrt{3}a \times 14a$ strip with irregular edges, for $\omega = 1.2$ at $t = 50$, 100, 200 (a) and $\omega = 2$ at $t = 10$, 30, 50 (b) (from the top to the bottom). The radius of circles is proportional to the spin-wave amplitude of $\sqrt{m_x^2 + m_y^2}$, and the colors encode the azimuthal angle ϕ shown by the color ring in the inset. (c) Spin-wave beam splitter: the snapshots of an in-coming spin wave at $t = 50$ (before entering into the domain wall), 100 (propagating along the domain wall), and 150 (after passing through the domain wall). The reddish (greenish) region is a domain with all spins pointing to $+z$ ($-z$) direction. The spin wave is generated by a microwave pulse of $\omega = 1.2$ with a duration of $\Delta t = 50$ at the site indicated by the black arrow on the bottom edge.

domain at $\omega = 1.2$, the spin wave must propagate along the domain wall to reach the top edge as shown in the middle panel of Fig. 4(c) at $t = 100$. On the top strip edge, the spin wave is split into two beams with one propagating leftwards in the reddish domain and the other one propagating rightwards in the greenish domain as shown in the lower panel of Fig. 4(c) at $t = 150$. Thus, it demonstrates a perfect spin-wave beam splitter that is still missing in the magnonics arsenal.

The results presented above do not include damping that exists in all realistic systems. It is easy to numerically include damping in Eq. (2). The physics are the same except spin waves decay exponentially during their propagation. For yttrium iron garnet, the damping of which can be as low as 10^{-5}, the decay length of a spin wave of 10 nm in wavelength could be of the order of millimeters, sufficient in many applications. Also, our results should be valid as long as the temperature is lower than the Curie temperature. Although noninteracting magnons are considered here, it is straightforward to include nonlinearity in our formulation so that one can investigate magnon-magnon interactions to consider other richer physics [38]. The model presented here could be realized by a properly arranged magnetic cluster array [39] if $\mathcal{F}$ is from the real dipole-dipole interaction and its long-range parts can be ignored. A more realistic realization of the pseudodipolar term can be originated from the spin-orbit interaction in some magnetic materials [31,32] that can be as strong as the conventional Heisenberg exchange. Thus, in principle, the predictions presented here can be tested experimentally. In fact, the detailed form of the pseudodipolar interaction is not important. One could have topologically protected spin waves as long as an exchange term can lead to band inversion similar to its electronic counterpart [4]. Furthermore, one will expect our system also exhibits a "spin-wave Hall effect" or a "magnon Hall effect" [9] since the magnon wave packages experience a Lorentz-like force [10] from the Berry curvature.

IV. CONCLUSION

In conclusion, ferromagnetic spins on a 2D honeycomb lattice can be topologically nontrivial when a proper NN exchange interaction exists. Like their electron counterpart, magnons (spin waves) in the topological states are gapped in the bulk with gapless edge chiral modes. The Chern numbers of spin-wave bands are nonzero, resulting in topologically protected and unidirectionally propagating edge spin waves that are robust against defects. Furthermore, the system can change from a topological trivial state (with zero Chern number for each band) into a topological nontrivial state by tuning the staggered anisotropies of the two sublattices. Based on the chiral spin-wave states, a magnetic domain wall can be used as a perfect spin-wave beam splitter.

ACKNOWLEDGMENTS

This work was supported by National Natural Science Foundation of China (Grant No. 11374249) and Hong Kong Research Grants Council (Grants No. 163011151 and No. 16301816). X.S.W. acknowledges support from University of Electronic Science and Technology of China.

[1] C. L. Kane and E. J. Mele, Phys. Rev. Lett. **95**, 146802 (2005).
[2] B. A. Bernevig, T. L. Hughes, and S.-C. Zhang, Science **314**, 1757 (2006).
[3] M. König, S. Wiedmann, C. Brüne, A. Roth, H. Buhmann, L. W. Molenkamp, X.-L. Qi, and S.-C. Zhang, Science **318**, 766 (2007).
[4] X.-L. Qi and S.-C. Zhang, Rev. Mod. Phys. **83**, 1057 (2011).
[5] C. L. Kane and T. C. Lubensky, Nat. Phys. **10**, 39 (2014).
[6] F. D. M. Haldane and S. Raghu, Phys. Rev. Lett. **100**, 013904 (2008).
[7] S. Fujimoto, Phys. Rev. Lett. **103**, 047203 (2009).

[8] H. Katsura, N. Nagaosa, and P. A. Lee, Phys. Rev. Lett. **104**, 066403 (2010).

[9] Y. Onose, T. Ideue, H. Katsura, Y. Shiomi, N. Nagaosa, and Y. Tokura, Science **329**, 297 (2010).

[10] R. Matsumoto and S. Murakami, Phys. Rev. Lett. **106**, 197202 (2011); R. Matsumoto, R. Shindou, and S. Murakami, Phys. Rev. B **89**, 054420 (2014).

[11] L. Zhang, J. Ren, J.-S. Wang, and B. Li, Phys. Rev. B **87**, 144101 (2013).

[12] M. Mochizuki, X. Z. Yu, S. Seki, N. Kanazawa, W. Koshibae, J. Zang, M. Mostovoy, Y. Tokura, and N. Nagaosa, Nat. Mater. **13**, 241 (2014).

[13] A. Mook, J. Henk, and I. Mertig, Phys. Rev. B **90**, 024412 (2014).

[14] M. Mena, R. S. Perry, T. G. Perring, M. D. Le, S. Guerrero, M. Storni, D. T. Adroja, Ch. Rüegg, and D. F. McMorrow, Phys. Rev. Lett. **113**, 047202 (2014).

[15] H. Lee, J. H. Han, and P. A. Lee, Phys. Rev. B **91**, 125413 (2015).

[16] R. Chisnell, J. S. Helton, D. E. Freedman, D. K. Singh, R. I. Bewley, D. G. Nocera, and Y. S. Lee, Phys. Rev. Lett. **115**, 147201 (2015).

[17] C.-E. Bardyn, T. Karzig, G. Refael, and T. C. H. Liew, Phys. Rev. B **93**, 020502(R) (2016).

[18] S. A. Owerre, J. Phys. Condens. Matter **28**, 386001 (2016).

[19] S. K. Kim, H. Ochoa, R. Zarzuela, and Y. Tserkovnyak, Phys. Rev. Lett. **117**, 227201 (2016).

[20] R. Shindou, J. I. Ohe, R. Matsumoto, S. Murakami, and E. Saitoh, Phys. Rev. B **87**, 174402 (2013).

[21] R. Shindou, R. Matsumoto, S. Murakami, and J. I. Ohe, Phys. Rev. B **87**, 174427 (2013).

[22] I. Lisenkov, V. Tyberkevych, A. Slavin, P. Bondarenko, B. A. Ivanov, E. Bankowski, T. Meitzler, and S. Nikitov, Phys. Rev. B **90**, 104417 (2014).

[23] S. O. Demokritov and A. N. Slavin, *Magnonics: From Fundamentals to Applications*, Topics in Applied Physics Vol. 125 (Springer, Berlin, 2013).

[24] D. Grundler, Nat. Phys. **11**, 438 (2015).

[25] B. Lenk, H. Ulrichs, F. Garbs, and M. Mnzenberg, Phys. Rep. **507**, 107 (2011).

[26] A. V. Chumak, V. I. Vasyuchka, A. A. Serga, and B. Hillebrands, Nat. Phys. **11**, 453 (2015).

[27] P. Yan, X. S. Wang, and X. R. Wang, Phys. Rev. Lett. **107**, 177207 (2011).

[28] X. S. Wang, P. Yan, Y. H. Shen, G. E. W. Bauer, and X. R. Wang, Phys. Rev. Lett. **109**, 167209 (2012).

[29] B. Hu and X. R. Wang, Phys. Rev. Lett. **111**, 027205 (2013).

[30] J. R. Eshbach and R. W. Damon, Phys. Rev. **118**, 1208 (1960).

[31] L. Shekhtman, O. Entin-Wohlman, and A. Aharony, Phys. Rev. Lett. **69**, 836 (1992).

[32] G. Jackeli and G. Khaliullin, Phys. Rev. Lett. **102**, 017205 (2009).

[33] T. L. Gilbert, IEEE. Trans. Magn. **40**, 3443 (2004).

[34] R. M. White, M. Sparks, and I. Ortenburger, Phys. Rev. **139**, A450 (1965).

[35] A. H. C. Neto, F. Guinea, N. M. R. Peres, K. S. Novoselov, and A. K. Gein, Rev. Mod. Phys. **81**, 109 (2009).

[36] J. E. Avron, R. Seiler, and B. Simon, Phys. Rev. Lett. **51**, 51 (1983).

[37] A. Bohm, A. Mostafazadeh, H. Koizumi, Q. Niu, and J. Zwanziger, *The Geometric Phase in Quantum Systems: Foundations, Mathematical Concepts, and Applications in Molecular and Condensed Matter Physics* (Springer, Berlin, 2003).

[38] A. L. Chernyshev and P. A. Maksimov, Phys. Rev. Lett. **117**, 187203 (2016).

[39] H.-H. Pan, H. Liu, J.-Z. Wang, J.-F. Jia, Q.-K. Xie, J.-L. Li, S. Qin, U. M. Mirsaidov, X. R. Wang, J. T. Markert, Z. Zhang, and C.-K. Shih, Nano Lett. **5**, 87 (2005).